Supporting Information

Complex Phase Behavior in Particle-Forming AB/AB′ Diblock Copolymer Blends with Variable Core Block Lengths

Aaron P. Lindsay,[1] Guo Kang Cheong,[1] Austin J. Peterson,[1] Steven Weigand,[3] Kevin D. Dorfman,[1] Timothy P. Lodge,[1,2] Frank S. Bates*[1]

[1]Department of Chemical Engineering and Materials Science and [2]Department of Chemistry, University of Minnesota, Minneapolis, MN 55455, USA

[3]DND-CAT Synchrotron Research Center, Northwestern University, APS/ANL Building 432-A004, 9700 South Cass Ave, Argonne, Illinois 60439, USA

*Corresponding Author: Frank S. Bates (bates001@umn.edu)

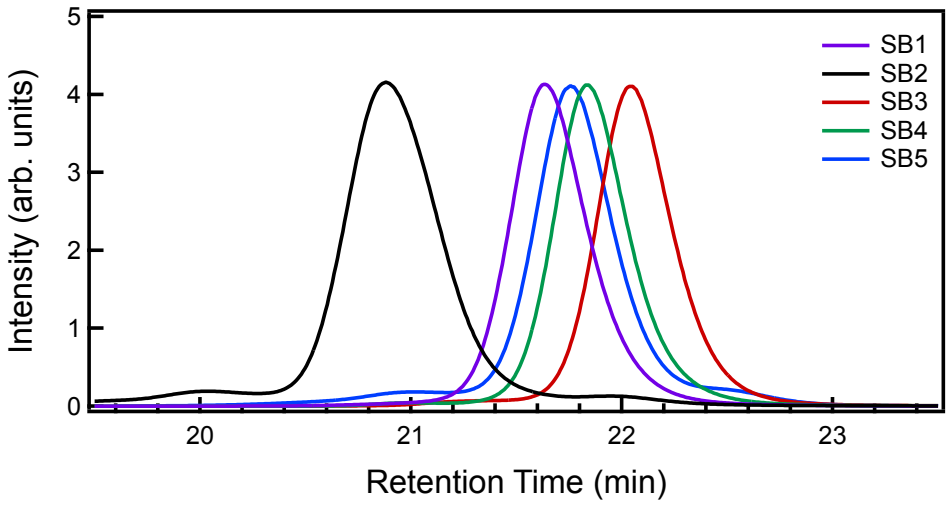

Figure S1. Size exclusion chromatography light scattering traces collected in tetrahydrofuran.

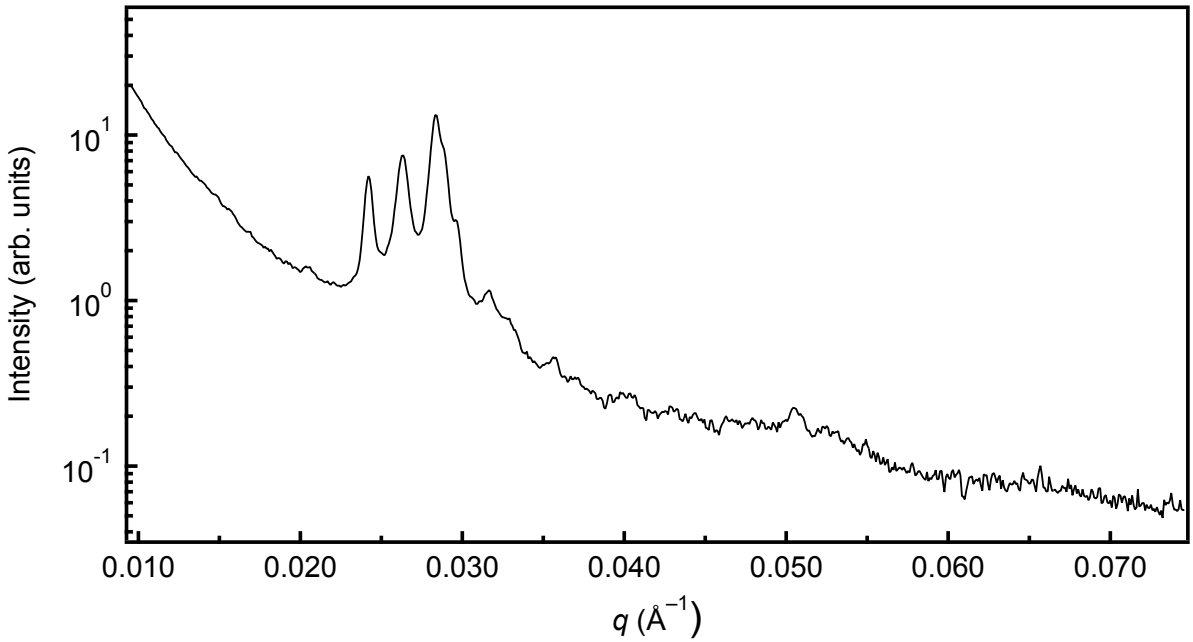

Figure S2. Extended 1D SAXS trace for the C14 Laves phase observed in SB1/SB2 blends with ϕ_2 = 0.075 at 150 ºC following the thermal processing outlined in Figure 2 and the main text. Indexing and residuals can be found in Table S1.

Table S1. Observed and calculated peak positions for the C14 Laves phase in Figures 2 and S2; data were collected from SB1/SB2 blends with $\phi_2 = 0.075$ at 150 ºC. Peak positions were calculated as $q_{hkl} = 2\pi\,[(4/3)\,(h^2 + hk + k^2)/a^2 + l^2/c^2]^{1/2}$ based on $P6_3/mmc$ space group symmetry with lattice parameters a = 520.0 Å and c = 847.5 Å.

Miller Indices (hkl)	q_{obs} (1/Å)	q_{calc} (1/Å)	% Residual ($\Delta q/\, q_{calc} \times 100$)
(100)	0.013948	0.013952	0.03
(002)	0.014846	0.014827	–0.13
(101)	0.015744	0.015800	0.35
(102)	0.020325	0.020359	0.17
(110)	0.024188	0.024166	–0.09
(103)	0.026292	0.026254	–0.14
(200)	–	0.027905	–
(112)	0.028319	0.028352	0.12
(201)	0.028858	0.028873	0.05
(004)	0.029577	0.029653	0.26
(202)	0.031643	0.031599	–0.14
(104)	0.032900	0.032772	–0.39
(203)	0.035685	0.035683	–0.01
(210)	0.036942	0.036914	–0.07

Table S2. Observed and calculated peak positions for the σ phase coexisting with HEX_C in Figures 3 and 4. Data were collected from an SB3/SB4 blend with $\phi_2 = 0.80$ at 150 ºC. Peak positions were calculated as $q_{hkl} = 2\pi\,[\,(h^2 + hk + k^2)/a^2 + l^2/c^2]^{1/2}$ based on $P4_2/mnm$ space group symmetry with lattice parameters a = 917.8 Å and c = 484.9 Å.

Miller Indices (hkl)	q_{obs} (1/Å)	q_{calc} (1/Å)	% Residual ($\Delta q/\, q_{calc} \times 100$)
(110)	–	0.009682	–
(200)	–	0.013692	–
(101)	–	0.014654	–
(210)	–	0.015308	–
(111)	–	0.016174	–
(220)	–	0.019363	–
(211)	0.020048	0.020055	0.04
(310)	0.021753	0.021649	–0.48
(221)	0.023369	0.023298	–0.30
(301)	0.024267	0.024283	0.07
(320)	0.024626	0.024684	0.23
(311)	0.025255	0.025230	–0.10
(002)	0.025917	0.025913	–0.02
(400)	0.027320	0.027384	0.23
(112)	–	0.027663	–
(321)	0.027858	0.027877	0.07
(410)	0.028217	0.028227	0.03
(330)	0.029025	0.029045	0.07
(202)	0.029295	0.029308	0.04
(212)	–	0.030097	–
(420)	–	0.030616	–
(411)	0.03109	0.031058	–0.10
(331)	0.031809	0.031804	–0.02
(222)	0.032347	0.032348	0.00
(421)	0.033155	0.033245	0.27
(312)	0.033694	0.033766	0.21
(430)	–	0.034230	–
(510)	–	0.034908	–
(322)	0.035849	0.035788	–0.17
(501)	0.036657	0.036600	–0.16
(520)	–	0.036867	–
(511)	0.037195	0.037235	0.11

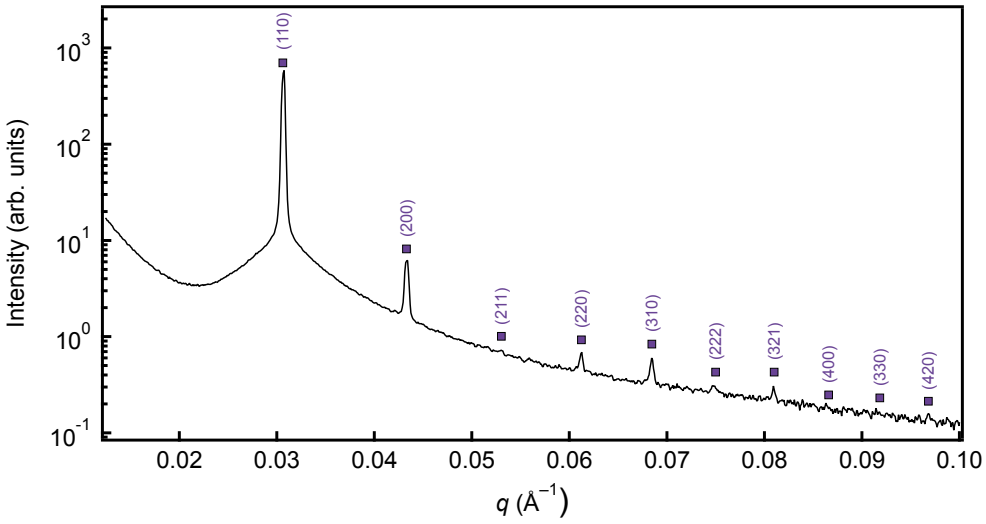

Figure S3. 1D SAXS trace collected from a SB3/SB4 blend with ϕ_2 = 0.80 following a 169 h anneal at 180 ºC. The trace is indexed to a BCC phase.

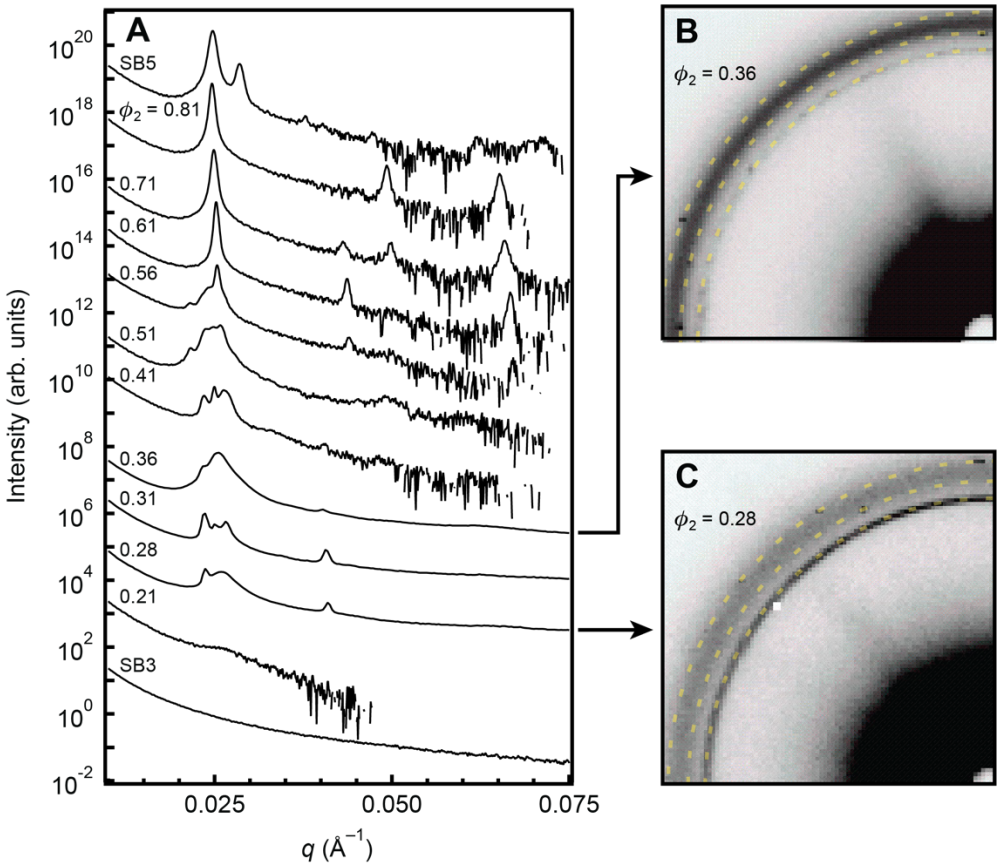

Figure S4. (A) 1D and (B,C) 2D SAXS data collected from SB3/SB5 blends following extended annealing (66-92 h) at 120 ºC. 2D SAXS data in B and C was collected following 92 h of annealing at 120 ºC. 2D data is indexed to the HCP phase (yellow dashed lines).

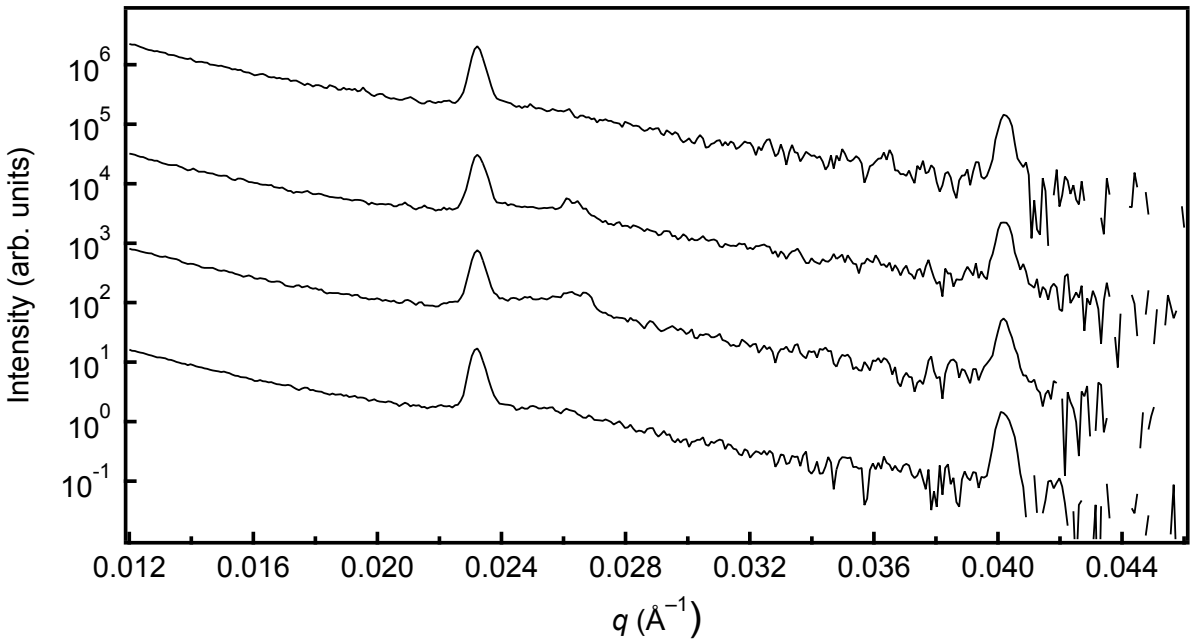

Figure S5. 1D SAXS traces collected from different locations on a SB3/SB5 blend with $\phi_2 = 0.31$ following 66 h of annealing at 150 ºC.

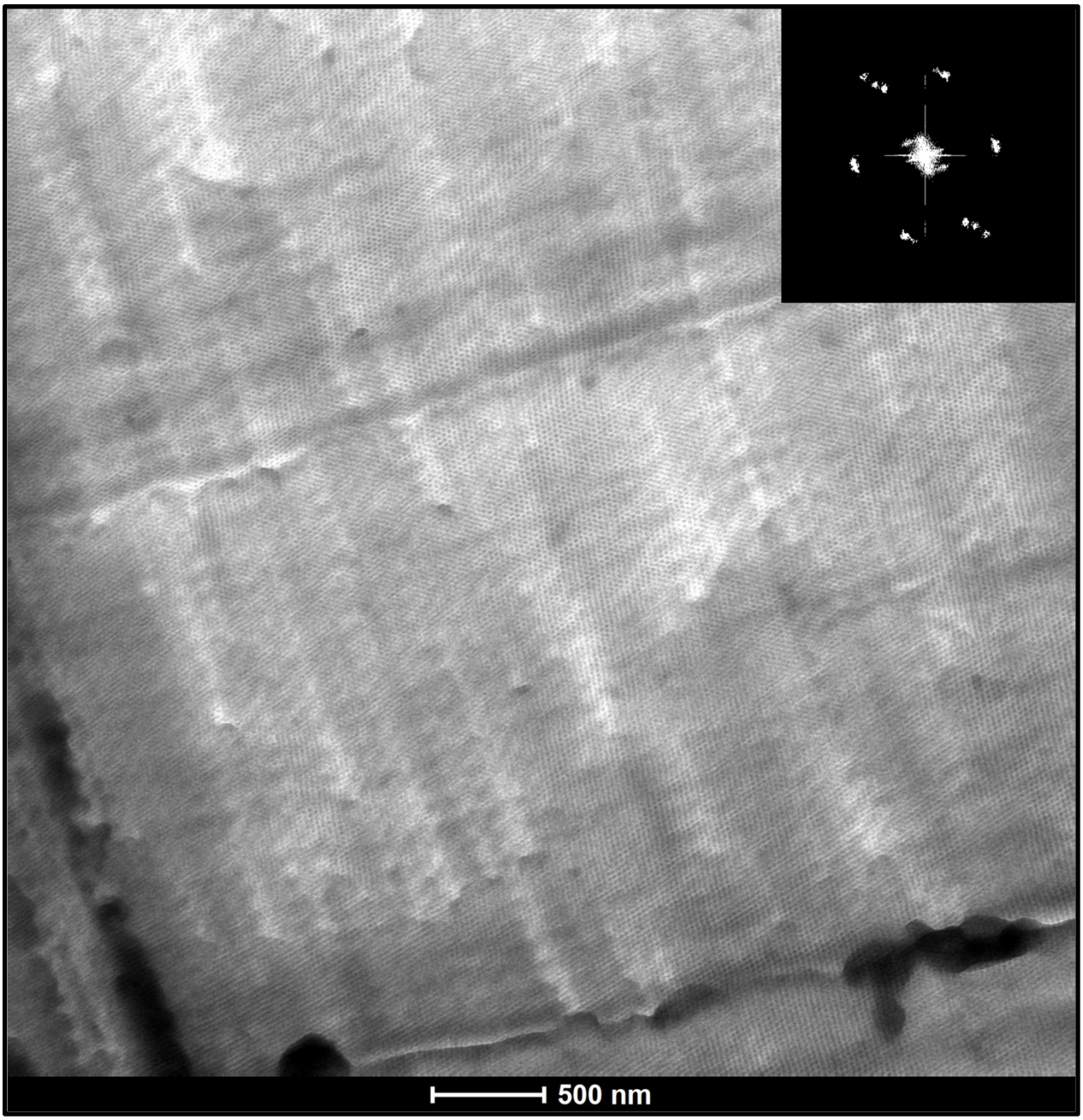

Figure S6. Transmission electron microscopy (TEM) micrograph collected from a thin (~70 nm) microtomed section of a SB3/SB5 blend with ϕ_2 = 0.31. Prior to microtoming, the sample was annealed for 66 h at 150 ºC, after which the SAXS patterns in Figures 5A,C and S5 were collected and the sample was vitrified in liquid nitrogen. The inset in the upper right corner is a Fourier transform of the image displaying the 6-fold rotation symmetry present over large areas.

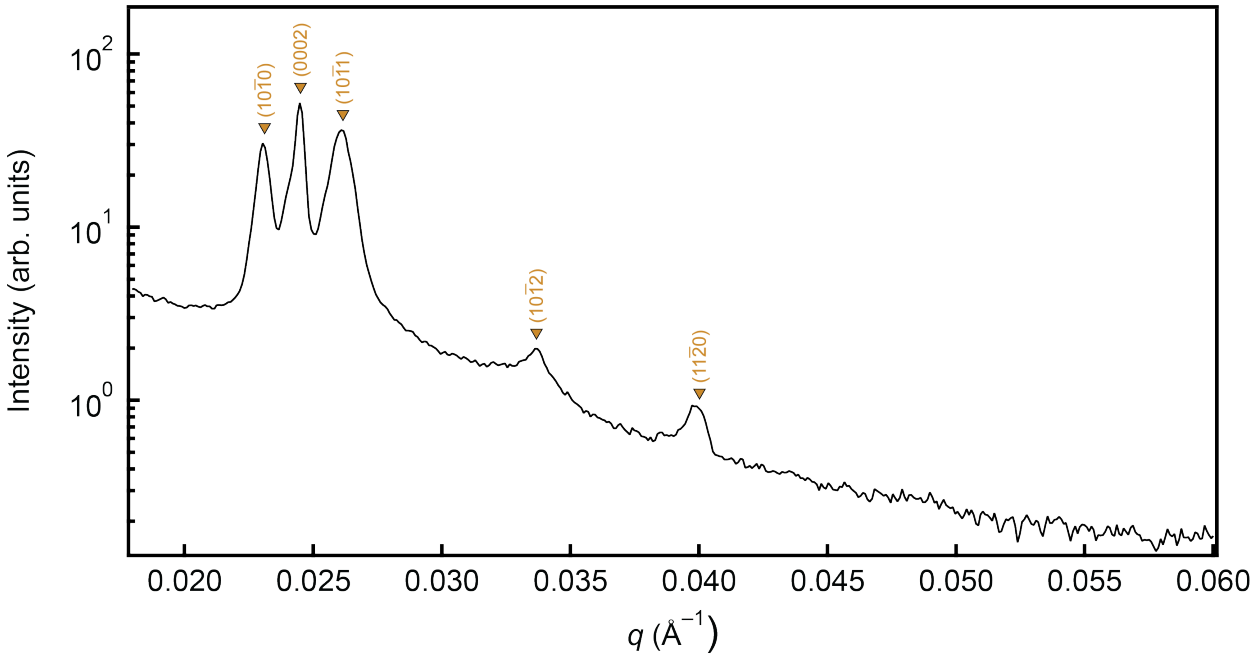

Figure S7. 1D SAXS trace collected from a SB3/SB5 blend with ϕ_2 = 0.41 following 92 h of annealing a 180 ºC. The trace is indexed to a HCP phase. Additional patterns can be found in Figures 5 and S9. Indexing and residuals can be found in Table S4.

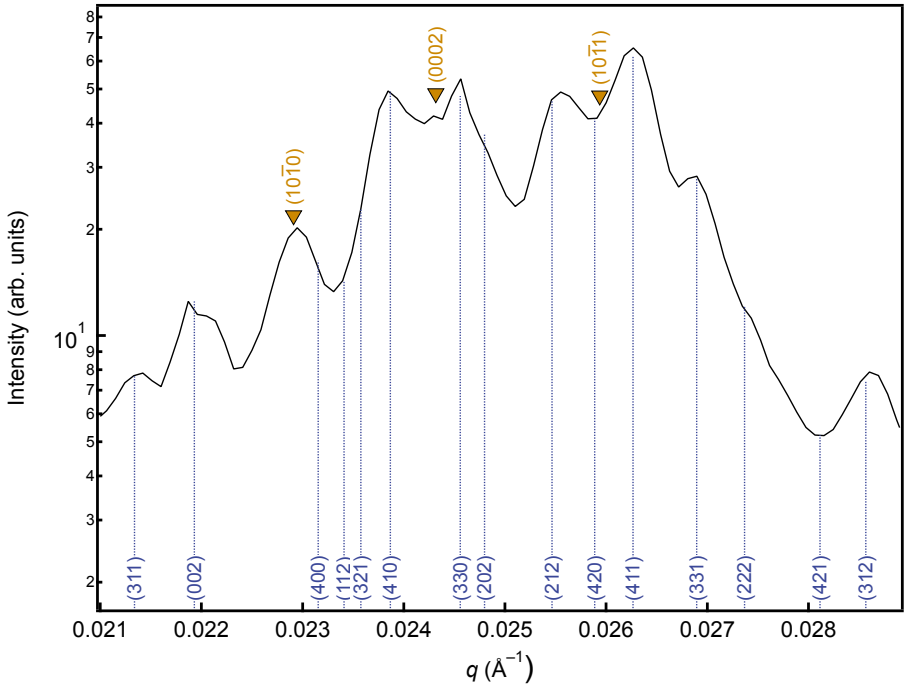

Figure S8. 1D SAXS trace collected from a SB3/SB5 blend with ϕ_2 = 0.46 after annealing at 180 ºC for 66 h. Lines and inverted triangles denote peaks associated with the σ and HCP phases, respectively. Indexing and residuals can be found in Table S3.

Table S3. Observed and calculated peak positions for the σ/HCP phase coexistence evidenced in Figures 5 and S10; data were collected from SB3/SB5 blends with ϕ_2 = 0.46 at 180 ºC. Peak positions for the HCP phase were calculated as $q_{hkl} = 2\pi\,[(4/3)\,(h^2 + hk + k^2)/a^2 + l^2/c^2]^{1/2}$ based on $P6_3/mmc$ space group symmetry with lattice parameters a = 316.7 Å and c = 517.1 Å. Peak positions for the σ phase were calculated as $q_{hkl} = 2\pi\,[(h^2 + k^2)/a^2 + l^2/c^2]^{1/2}$ based on $P4_2/mnm$ space group symmetry with lattice parameters a = 1085.5 Å and c = 573.0 Å.

Miller Indices (*hkil*) or (*hkl*)	q_{obs} (1/Å)	q_{calc} (1/Å)	% Residual ($\Delta q/\, q_{calc} \times 100$)
		HCP	
$(10\bar{1}0)$	0.022946	0.022910	–0.16
(0002)	0.024293	0.024300	0.03
$(10\bar{1}1)$	–	0.025933	–0.26
$(10\bar{1}2)$	0.033539	0.033397	–0.43
$(11\bar{2}0)$	0.039643	0.039682	0.10
$(10\bar{1}3)$	–	0.043052	–
$(20\bar{2}0)$	0.046016	0.045820	–0.43
$(11\bar{2}2)$	0.046555	0.046531	–0.05
$(20\bar{2}1)$	0.047363	0.047404	0.09
(0004)	0.048799	0.048599	–0.41
$(20\bar{2}2)$	0.051761	0.051865	0.20
		σ	
(211)	0.016932	0.016964	0.19
(310)	0.018279	0.018304	0.14
(221)	0.019625	0.019705	0.40
(301)	0.020613	0.020537	–0.37
(320)	–	0.020870	–
(311)	0.021331	0.021337	0.03
(002)	0.021959	0.021931	–0.13
(400)	–	0.023153	–
(112)	–	0.023409	–
(321)	–	0.023575	–
(410)	0.023844	0.023866	0.09
(330)	0.024562	0.024558	–0.02
(202)	0.024832	0.024799	–0.13
(212)	0.02555	0.025465	–0.33
(420)	–	0.025886	–
(411)	0.026268	0.026264	–0.01
(331)	0.026896	0.026895	–0.01

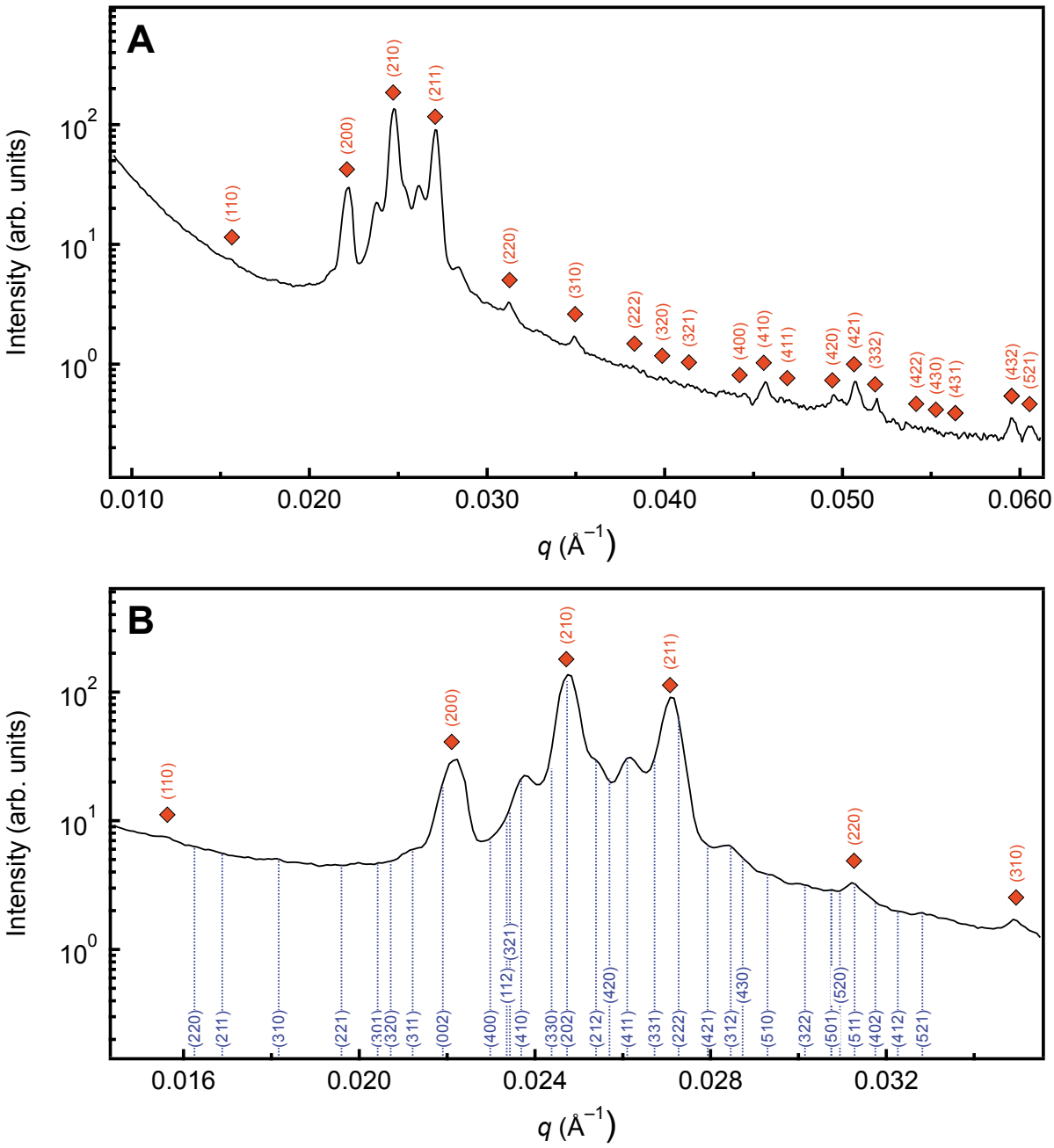

Figure S9. 1D SAXS trace collected from a SB3/SB5 blend with $\phi_2 = 0.51$ after annealing at 180 ºC for 66 h. Lines and diamonds denote peaks associated with σ and A15 phases, respectively. Indexing and residuals can be found in Table S6.

Table S4. Observed and calculated peak positions for the A15/σ phase coexistence evidenced in Figures 5 and S11; data were collected from SB3/SB5 blends with $\phi_2 = 0.51$ at 180 ºC. Peak positions for the A15 phase were calculated as $q_{hkl} = 2\pi\,[(h^2 + k^2 + l^2)\,/a^2]^{1/2}$ based on $Pm\bar{3}n$ space group symmetry with a lattice parameter of a = 568.5 Å. Peak positions for the σ phase were calculated as $q_{hkl} = 2\pi\,[(h^2 + k^2)/a^2 + l^2/c^2]^{1/2}$ based on $P4_2/mnm$ space group symmetry with lattice parameters a = 1093.3 Å and c = 573.7 Å.

Miller Indices (*hkl*)	q_{obs} (1/Å)	q_{calc} (1/Å)	% Residual ($\Delta q/\, q_{calc} \times 100$)
		A15	
(110)	0.015586	0.015630	0.28
(200)	0.022228	0.022104	–0.56
(210)	0.024742	0.024713	–0.12
(211)	0.027165	0.027072	–0.34
(220)	0.031205	0.031260	0.18
(310)	0.034885	0.034950	0.19
(222)	0.038207	0.038285	0.20
(320)	0.039733	0.039849	0.29
(321)	0.041348	0.041353	0.01
(400)	0.0444	0.044208	–0.43
(410)	0.045657	0.045569	–0.19
(411)	0.047004	0.046890	–0.24
(420)	0.049517	0.049426	–0.18
(421)	0.050684	0.050647	–0.07
(332)	0.051941	0.051839	–0.20
		σ	
(410)	0.023754	0.023695	–0.25
(330)	–	0.024382	–
(202)	–	0.024735	–
(212)	0.02546	0.025394	–0.26
(420)	–	0.025701	–
(411)	0.026178	0.026103	–0.29
(331)	–	0.026728	–
(222)	–	0.027275	–
(421)	–	0.027937	–
(312)	0.028422	0.028460	0.13
(430)	–	0.028734	–
(510)	0.02941	0.029303	–0.36
(322)	0.030038	0.030150	0.37

Table S5. Observed and calculated peak positions for the QC evidenced in Figures 5 and S12; data were collected from SB3/SB5 blends with $\phi_2 = 0.51$ at 150 ºC. Peak positions were calculated as described by Iwami and Ishimasa [1] based on a $P12_6/mmc$ space group symmetry, a tiling edge length $a = 572.9$ Å, and a periodicity of $c = 575.6$ Å.

Miller Indices ($a_1\, a_2\, a_3\, a_4\, a_5$)	q_{obs} (1/Å)	q_{calc} (1/Å)	% Residual ($\Delta q/\, q_{calc} \times 100$)
(11000)	–	0.012233	–
(00002)	0.021780	0.021832	0.24
(12100)	0.023844	0.023633	–0.89
(01102)	0.024921	0.025026	0.42
$(220\bar{1}1)$	0.025999	0.026032	0.13
(11102)	0.028063	0.027856	–0.74
(12202)	–	0.036531	–
(00004)	0.043664	0.043664	0.00
(01104)	0.045298	0.045345	0.10

Table S6. Observed and calculated peak positions for the A15 phase coexisting with HEX_C evidenced in Figures 5 and S13; data was collected from SB3/SB5 blends with $\phi_2 = 0.56$ at 180 ºC. Peak positions for the A15 phase were calculated as $q_{hkl} = 2\pi\, [(h^2 + k^2 + l^2)\, /a^2]^{1/2}$ based on $Pm\bar{3}n$ space group symmetry with a lattice parameter of $a = 577.0$ Å.

Miller Indices (hkl)	q_{obs} (1/Å)	q_{calc} (1/Å)	% Residual ($\Delta q/\, q_{calc} \times 100$)
(110)	–	0.015400	–
(200)	0.021753	0.021779	0.12
(210)	0.024357	0.024349	–0.03
(211)	0.026601	0.026673	0.27
(220)	–	0.030800	–

Calculation of mean particle radii:

For a periodic particle packing, the mean particle radius $\langle R \rangle$ can be calculated as:

$$\langle R \rangle = \left(\frac{3 V_{\mathrm{UC}}}{4\pi \rho_{\mathrm{P,UC}}} \right)^{1/3} \tag{S1}$$

where V_{UC} is the unit cell volume, which can be readily determined *via* SAXS, and $\rho_{\mathrm{P,UC}}$ is the number of particles per unit cell set by the packing. In the most general form, unit cell volume can be calculated as:

$$V_{\mathrm{UC}} = a\, b\, c \left(1 - \cos^2\alpha - \cos^2\beta - \cos^2\gamma + 2\cos\alpha \cos\beta \cos\gamma\right)^{1/2} \tag{S2}$$

where a, b, and c are lattice constants and the angles α, β, and γ are lattice parameters. These values are determined from SAXS from the relations:

$$q_{\mathrm{hkl,cubic}} = 2\pi \left(\frac{\left(h^2 + \mathrm{k}^2 + l^2\right)}{a^2} \right)^{1/2} \tag{S3}$$

$$q_{\mathrm{hkl,hexagonal}} = 2\pi \left(\frac{4\left(h^2 + hk + \mathrm{k}^2\right)}{3a^2} + \frac{l^2}{c^2} \right)^{1/2} \tag{S4}$$

$$q_{\mathrm{hkl,tetragonal}} = 2\pi \left(\frac{\left(h^2 + \mathrm{k}^2\right)}{a^2} + \frac{l^2}{c^2} \right)^{1/2} \tag{S5}$$

for cubic, hexagonal, or tetragonal lattices, where q_{hkl} is the scattering wavevector for plane (*hkl*), $\alpha = \beta = \gamma = 90^{\circ}$ for a cubic or tetragonal lattice, and $\alpha = \beta = 90^{\circ}$ and $\gamma = 120^{\circ}$ for a hexagonal lattice.

From these relations, $\langle R \rangle$ can be calculated for the phases observed in this work as:

$$\langle R \rangle_{\mathrm{BCC}} = R_{\mathrm{BCC}} = \frac{3^{1/3} 2^{1/2} \pi^{2/3}}{q_{110}} \tag{S6}$$

$$\langle R \rangle_{\mathrm{FCC}} = R_{\mathrm{FCC}} = \frac{3^{5/6} \pi^{2/3}}{2^{1/3}\, q_{111}} \tag{S7}$$

$$\langle R\rangle_{\mathrm{HCP}} = R_{\mathrm{HCP}} = \frac{2^{2/3}\pi^{2/3}(c/a)^{1/3}}{q_{10\bar{1}0}} \tag{S8}$$

$$\langle R\rangle_{\sigma} = \frac{2\pi^{2/3}}{5^{1/3}(c/a)^{2/3}q_{002}} \tag{S9}$$

$$\langle R\rangle_{\mathrm{A15}} = \frac{3^{1/3}\pi^{2/3}}{2^{1/6}q_{110}} \tag{S10}$$

$$\langle R\rangle_{\mathrm{C14}} = \frac{2^{1/3}\pi^{2/3}(c/a)^{1/3}}{3^{1/3}q_{10\bar{1}0}} \tag{S11}$$

Owing to a lack of translational symmetry, $\langle R\rangle$ for a dodecagonal quasicrystal (QC) or a liquid-like packing (LLP) can only be estimated. For a QC, this is best done by taking the (00002) reflection as the σ q_{002} peak owing to the close structural relationship between the two phases and the invariance of this reflection on transition to the σ phase.[2,3] For LLP the principal reflection can be taken as the q_{110} peak of the BCC phase by a similar argument. On calculating $\langle R\rangle$, the core radius can be calculated as:

$$\langle R_{\mathrm{core}}\rangle = f_{\mathrm{core}}{}^{1/3}\langle R\rangle \tag{S12}$$

where f_{core} is volume fraction of the core domain assuming complete segregation of both blocks. This core radius can then be used to calculate the underlying spherical form factor.

A similar strategy can be used to calculate the radius of cylinders in the hexagonally-packed cylinder ($\mathrm{HEX_C}$) phase. However, the functional form changes slightly owing to periodicity in only two dimensions. $\langle R\rangle$ is instead calculated as:

$$R_{\mathrm{cyl}} = \left(\frac{A_{\mathrm{UC}}}{\pi\rho_{\mathrm{C,UC}}}\right)^{1/2} \tag{S13}$$

where A_{UC} is the unit cell area, which can be readily determined *via* SAXS, and $\rho_{C,UC} = 1$ is the number of cylinders per unit cell. The unit cell area can be calculated as:

$$A_{UC} = \frac{3^{1/2}a^2}{2} \tag{S14}$$

The lattice parameter a is determined from SAXS according to the relation:

$$q_{hk,hexagonal2D} = 2\pi\left(\frac{4\left(h^2 + hk + k^2\right)}{3a^2}\right)^{1/2} \tag{S15}$$

From these equations, $\langle R \rangle$ can be calculated for the HEX_C phase as:

$$R_{cyl} = \frac{2^{3/2}\pi^{1/2}}{3^{1/4}q_{10}} \tag{S16}$$

On calculating R_{cyl}, the cylinder core radius can then be calculated as:

$$R_{core,cyl} = f_{core}^{1/2}R_{cyl} \tag{S17}$$

where f_{core} is again the volume fraction of the core domain assuming complete segregation of both blocks. This core radius can then be used to calculate the underlying cylindrical form factor.

Dispersity:

Core block dispersity $Đ \approx 1.12$ was estimated for SB3/SB4 blends with $\phi_2 = 0.80$ approximating the constituent diblock copolymers as monodisperse via the relation:

$$Đ = \frac{M_w}{M_n} \tag{S18}$$

where M_w and M_n are the weight- and number-average block molecular weights calculated as:

$$M_n = x_1 M_{n,1} + x_2 M_{n,2} \tag{S19}$$

$$M_w = \frac{x_1 M_{n,1}^2 + x_2 M_{n,2}^2}{x_1 M_{n,1} + x_2 M_{n,2}} \tag{S20}$$

where values of M_n for each block and polymer can be found in Table S1 and x_i is the mole fraction of copolymer *i* in the core domain. A similar approach can be used to estimate the dispersity of the corona as $Đ \approx 1.001$. Notably, this approach only provides an estimate and neglects the dispersity of each polymer, each determined via size exclusion chromatography (SEC) to be $Đ \approx 1.01$.

To compare this value with previously investigated 1,4-polyisoprene-*block*-poly(±-lactide) (IL) diblock copolymers, we assume a I precursor dispersity of 1.06, a reasonable estimate for low molecular weight I synthesized *via* anionic polymerization,[4] and independent block dispersities. Using the rule for the sum of variances of statistical distributions (*i.e.*, $Đ_{PIPLA} = w_{PI}^2(Đ_{PI} - 1) + w_{PLA}^2(Đ_{PLA} - 1) + 1$, where w_i is the mass fraction of block i), it can be found that many of the σ-forming IL diblock copolymers reported in the literature likely had core (L) block dispersities greater than the $Đ_{core} = 1.2$ we found in this work to be sufficient to drive σ-formation .[5–12] It should be noted that the accuracy of such calculations is limited by that of the assumed I precursor dispersity and the resolution of the instruments used for dispersity measurements.[13] However, there are several reasons one might anticipate a higher dispersity for the second block. First, ring-opening polymerization of lactides generally results in higher dispersity (~1.1–2.0) than anionic polymerization of isoprene (< 1.1).[5,14,15] Second, it is anticipated that some fraction of PI precursor will be present in the final diblock copolymer due to a combination of early termination,

incomplete reinitiation, and challenges inherent to purification.[13] Third, when considering the low molecular weight of these polymers, generally characterized by an average block length of 45 isoprene and 6 lactide monomer units, it is clear that the loss or gain of only a few lactide monomer units over the course of the polymerization would have a dramatic effect on the block dispersity.

Self-consistent mean-field theory (SCFT):

Calculations based on self-consistent mean-field theory were performed using the open-source Polymer Self-Consistent Field software package (PSCF).[16] We performed binary blend canonical ensemble calculations at $N_2/N_1 = 1.4$, $N_{B,1} = N_{B,2}$, $f_{A,1} = 0.12$, $f_{A,2} = 0.38$ and a conformational asymmetry of $\varepsilon = b_B/b_S$ (v_S/v_B) = 1.7. Note this differs modestly from experiments, where $f_{A,2}$ = 0.388, but is within experimental error and, thus, has a negligible impact on the applicability of the calculations to the experimental results. We scanned a range of χN (20–30) and ϕ_2 (0–1), mimicking the parameter space explored experimentally. The candidate phases tested in the canonical ensemble calculations include the body-centered cubic (BCC), face-centered cubic (FCC), hexagonally close-packed (HCP), hexagonally-packed cylinder (HEX_C), double gyroid (GYR), and disordered (DIS) phases as well as the Frank–Kasper (FK) σ, A15, C14, and C15 phases. SCFT calculations were performed using a grid size of 64×64×64 for the three-dimensional structures except for the σ and two-dimensional HEX_C phases, which were performed at a grid size of 96×96×48 and 64×64, respectively. Calculations were performed with a contour length step size of $\Delta s = 0.01$ and a convergence criterion of 10^{-5} as defined by Arora *et al.*[17] As shown in Figure S10, the free energies were almost degenerate at $\phi_2 = 0.15$ and 0.25. To better resolve the phase behavior at those compositions, we repeated the calculations using a more stringent convergence criterion of 10^{-6}. Figure S11 shows the results under this stricter convergence criterion, revealing that C15 and HCP phases offer the lowest free energy at low ϕ_2. Then, we performed grand canonical ensemble calculations between neighboring phases to resolve phase coexistence. Further calculation details can be found elsewhere.[18]

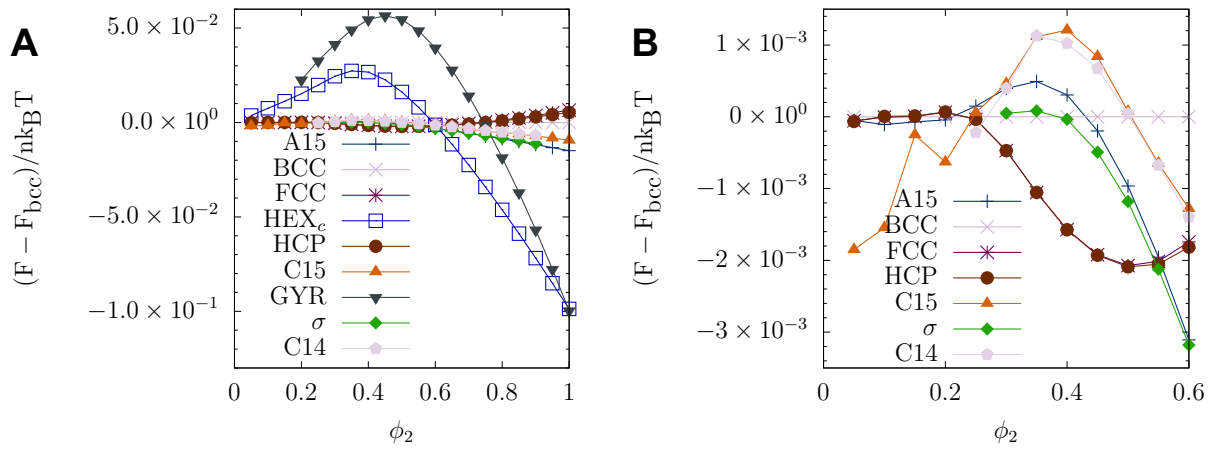

Figure S10. Normalized free energy relative to BCC *versus* ϕ_2 at $\chi N = 28$ for (A) all studied phases and (B) only particle phases.

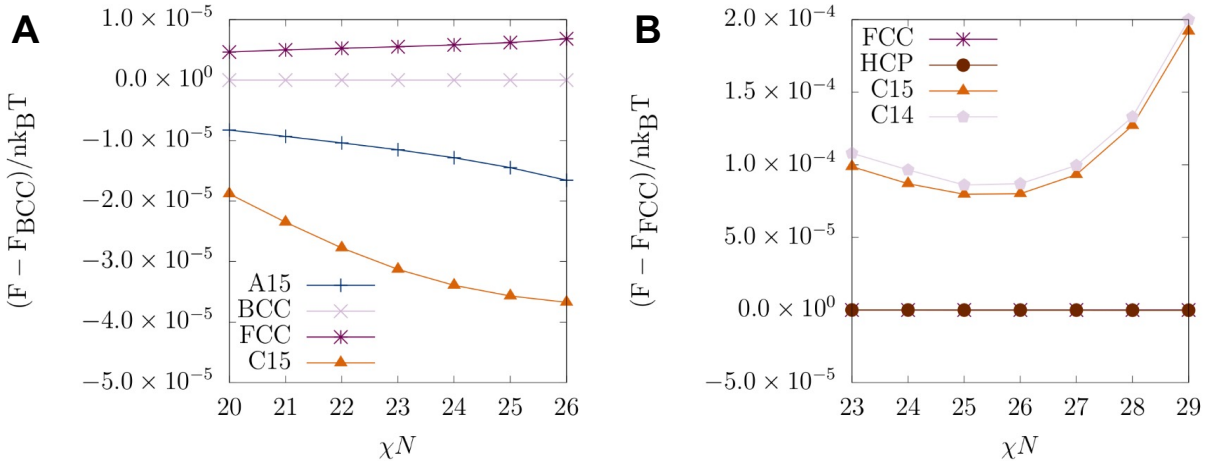

Figure S11. Normalized free energy relative to (A) BCC and (B) FCC *versus* χN at (A) $\phi_2 = 0.15$ and (B) $\phi_2 = 0.25$ for select phases under the more stringent convergence criterion of 10^{-6}.

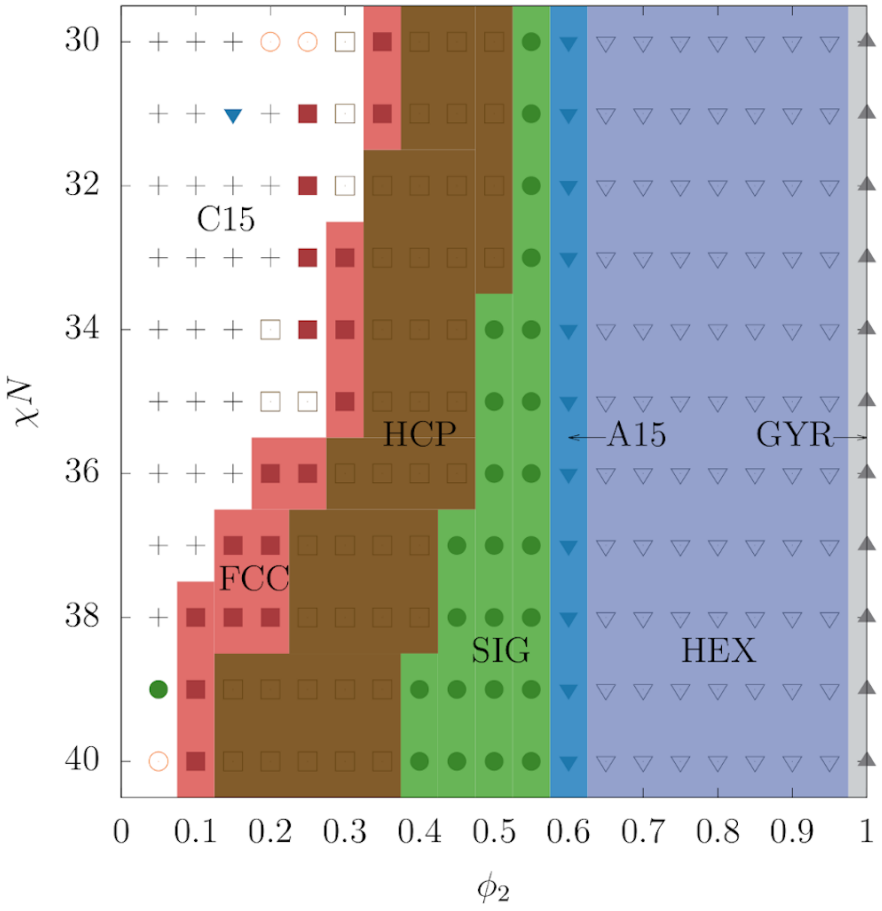

Figure S12. Binary blend phase diagram generated from canonical ensemble SCFT calculations over an extended range of χN ($N_2/N_1 = 1.4$, $N_{S,1} = N_{S,2}$, $f_{B,1} = 0.12$, and $f_{B,2} = 0.38$). Symbols correspond to the double gyroid (gray ▲), hexagonally-packed cylinder (purple ▽), A15 (blue ▼), σ (green ●), hexagonal close-packed □), face-centered cubic (red ■), C14 (orange ○), and C15 phases (black ＋).

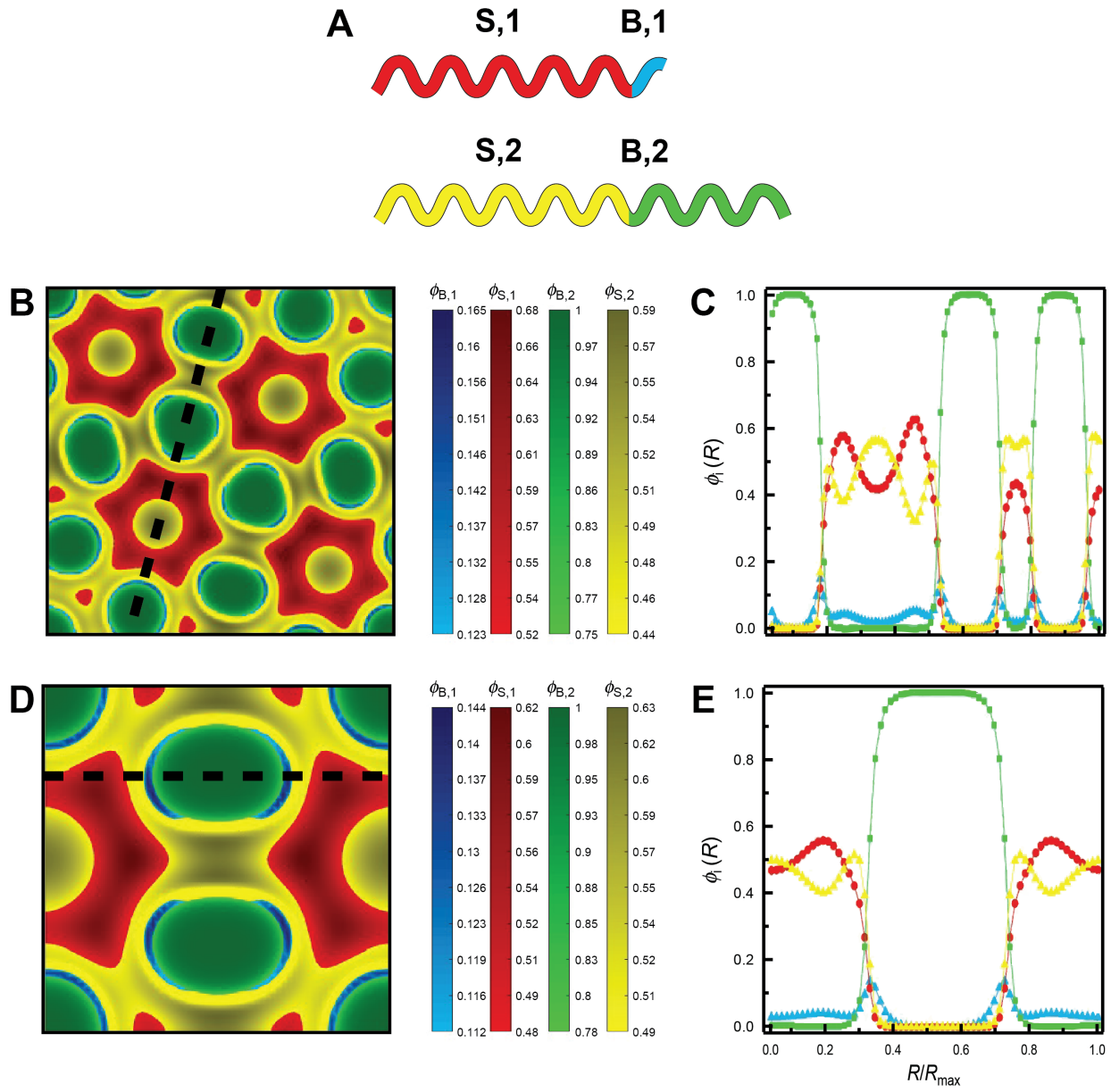

Figure S13. (B,D) Composition maps and (C,E) 1D composition profiles for the (B,C) σ and (D,E) A15 phases in the (001) planes. Data were calculated *via* SCFT for SB3/SB5 blends with (B,C) ϕ_2 = 0.55 and (D,E) 0.60 at $\chi\langle N\rangle$ = 30. ϕ_i is the volume fraction of block i at each position. R/R_{max} is the nondimensional distance along the dashed lines in (B,D), where 0 corresponds to the (C) bottom or (E) left edge of the composition map. The schematic in (A) shows the relative copolymer block lengths. Blue and red shading correspond to the B and S blocks of SB3, whereas green and yellow shading correspond to the B and S blocks of SB5, respectively.

References

(1) Iwami, S.; Ishimasa, T. Dodecagonal Quasicrystal in Mn-Based Quaternary Alloys Containing Cr, Ni and Si. *Philos. Mag. Lett.* **2015**, *95*, 229–236. https://doi.org/10.1080/09500839.2015.1038332.

(2) Lindsay, A. P.; Jayaraman, A.; Peterson, A. J.; Mueller, A. J.; Weigand, S.; Mahanthappa, M. K.; Lodge, T. P.; Bates, F. S. Reevaluation of Poly(Ethylene- Alt -Propylene)- Block -Polydimethylsiloxane Phase Behavior Uncovers Topological Close-Packing and Epitaxial Quasicrystal Growth. *ACS Nano* **2021**, *ASAP Article*. https://doi.org/10.1021/acsnano.1c02420.

(3) Lindsay, A. P.; Lewis, R. M.; Lee, B.; Peterson, A. J.; Lodge, T. P.; Bates, F. S. A15, σ, and a Quasicrystal: Access to Complex Particle Packings via Bidisperse Diblock Copolymer Blends. *ACS Macro Lett.* **2020**, *9*, 197–203. https://doi.org/10.1021/acsmacrolett.9b01026.

(4) Schmidt, S. C.; Hillmyer, M. A. Morphological Behavior of Model Poly(Ethylene-Alt-Propylene)-b-Polylactide Diblock Copolymers. *J. Polym. Sci. Part B Polym. Phys.* **2002**, *40*, 2364–2376. https://doi.org/10.1002/polb.10291.

(5) Lynd, N. A.; Hillmyer, M. A. Influence of Polydispersity on the Self-Assembly of Diblock Copolymers. *Macromolecules* **2005**, *38*, 8803–8810. https://doi.org/10.1021/ma051025r.

(6) Cooke, D. M.; Shi, A.-C. Effects of Polydispersity on Phase Behavior of Diblock Copolymers. *Macromolecules* **2006**, *39*, 6661–6671. https://doi.org/10.1021/ma060717s.

(7) Lee, S.; Bluemle, M. J.; Bates, F. S. Discovery of a Frank-Kasper σ Phase in Sphere-Forming Block Copolymer Melts. *Science* **2010**, *330*, 349–353. https://doi.org/10.1126/science.1195552.

(8) Gillard, T. M.; Lee, S.; Bates, F. S. Dodecagonal Quasicrystalline Order in a Diblock

Copolymer Melt. *Proc. Natl. Acad. Sci. U. S. A.* **2016**, *113*, 5167–5172. https://doi.org/10.1073/pnas.1601692113.

(9) Lee, S.; Leighton, C.; Bates, F. S. Sphericity and Symmetry Breaking in the Formation of Frank-Kasper Phases from One Component Materials. *Proc. Natl. Acad. Sci. U. S. A.* **2014**, *111*, 17723–17731. https://doi.org/10.1073/pnas.1408678111.

(10) Schulze, M. W.; Lewis, R. M.; Lettow, J. H.; Hickey, R. J.; Gillard, T. M.; Hillmyer, M. A.; Bates, F. S. Conformational Asymmetry and Quasicrystal Approximants in Linear Diblock Copolymers. *Phys. Rev. Lett.* **2017**, *118*, 207801. https://doi.org/10.1103/PhysRevLett.118.207801.

(11) Kim, K.; Arora, A.; Lewis, R. M.; Liu, M.; Li, W.; Shi, A. C.; Dorfman, K. D.; Bates, F. S. Origins of Low-Symmetry Phases in Asymmetric Diblock Copolymer Melts. *Proc. Natl. Acad. Sci. U. S. A.* **2018**, *115*, 847–854. https://doi.org/10.1073/pnas.1717850115.

(12) Kim, K.; Schulze, M. W.; Arora, A.; Lewis, R. M.; Hillmyer, M. A.; Dorfman, K. D.; Bates, F. S. Thermal Processing of Diblock Copolymer Melts Mimics Metallurgy. *Science* **2017**, *356*, 520–523. https://doi.org/10.1126/science.aam7212.

(13) Hiemenz, P. C.; Lodge, T. P. *Polymer Chemistry*, 2nd Editio.; CRC Press: Boca Raton, 2007.

(14) Dechy-Cabaret, O.; Martin-Vaca, B.; Bourissou, D. Controlled Ring-Opening Polymerization of Lactide and Glycolide. *Chem. Rev.* **2004**, *104*, 6147–6176. https://doi.org/10.1021/CR040002S.

(15) Schmidt, S. C.; Hillmyer, M. A. Synthesis and Characterization of Model Polyisoprene−Polylactide Diblock Copolymers. *Macromolecules* **1999**, *32*, 4794–4801. https://doi.org/10.1021/MA9900277.

(16) Arora, A.; Qin, J.; Morse, D. C.; Delaney, K. T.; Fredrickson, G. H.; Bates, F. S.; Dorfman, K. D. Broadly Accessible Self-Consistent Field Theory for Block Polymer Materials Discovery. *Macromolecules* **2016**, *49*, 4675–4690. https://doi.org/10.1021/acs.macromol.6b00107.

(17) Arora, A.; Morse, D. C.; Bates, F. S.; Dorfman, K. D. Accelerating Self-Consistent Field Theory of Block Polymers in a Variable Unit Cell. *J. Chem. Phys.* **2017**, *146*, 244902. https://doi.org/10.1063/1.4986643.

(18) Liu, M.; Qiang, Y.; Li, W.; Qiu, F.; Shi, A. C. Stabilizing the Frank-Kasper Phases via Binary Blends of AB Diblock Copolymers. *ACS Macro Lett.* **2016**, *5*, 1167–1171. https://doi.org/10.1021/acsmacrolett.6b00685.